Thin Solid Films 520 (2012) 4590–4594

Contents lists available at SciVerse ScienceDirect

Thin Solid Films

journal homepage: www.elsevier.com/locate/tsf

Raman spectroscopic and X-ray diffraction investigations of epitaxial $BiCrO_3$ thin films

Andreas Talkenberger [a,*], Cameliu Himcinschi [a], Torsten Weißbach [a], Kannan Vijayanandhini [b], Ionela Vrejoiu [b], Christian Röder [a], David Rafaja [c], Jens Kortus [a]

[a] Institute of Theoretical Physics, TU Bergakademie Freiberg, Leipziger Str. 23, D-09596 Freiberg, Germany
[b] Max Planck Institute of Microstructure Physics, Weinberg 2, D-06120 Halle, Germany
[c] Institute of Materials Science, TU Bergakademie Freiberg, Gustav-Zeuner-Str. 5, D-09596 Freiberg, Germany

ARTICLE INFO

Article history:
Received 31 May 2011
Received in revised form 30 August 2011
Accepted 23 October 2011
Available online 10 November 2011

Keywords:
$BiCrO_3$
Multiferroic thin films
XRD
Raman spectroscopy

ABSTRACT

Epitaxial $BiCrO_3$ thin films were grown onto $NdGaO_3$ (110)- and $(LaAlO_3)_{0.3}$-$(Sr_2AlTaO_6)_{0.7}$ (100)-oriented substrates by pulsed laser deposition. High resolution X-ray diffraction and pole figure measurements were performed in order to obtain information about the crystal structure of the films, about their quality and about the mutual crystallographic orientation between the films and the substrates. The monoclinic (111) plane of $BiCrO_3$ was found out to be parallel to the substrate surface. The epitaxial relation between films and substrates was verified by using polarisation dependent Raman spectroscopic experiments and theoretical calculations based on symmetry.

1. Introduction

Multiferroic epitaxial thin films are of strong research interest due to their potential applications, such as in memory devices [1–3]. For applications the fabrication of high-quality epitaxial thin films and a fundamental understanding of their physical properties are needed.

Among the candidates for multiferroic thin film materials the Bi-based magnetic transition metal perovskites, especially $BiFeO_3$, are on great interest [4,5]. Another interesting potential candidate is $BiCrO_3$ (BCO). BCO was first synthesised by Sugawara and Lida [6] in 1965 and shows a monoclinic crystal structure at room temperature with C2/c symmetry and phase transition to an orthorhombic crystal system above 420 K [7,8]. Recently, a third stable phase in epitaxial strained BCO films similar to a superstructure closely related to the C2/c monoclinic form was observed [9]. Concerning the magnetic and dielectric properties, bulk BCO shows a long-range antiferromagnetic order below $T_N = 109$ K [10] with weak ferromagnetism due to the canting of the Cr spins [11] and possesses an antiferroelectric order up to the structural transition temperature at around 410 K as proposed by Kim [12]. Raman spectroscopy is a non-destructive method which found increasing application in the characterisation of multiferroic thin film materials because of its sensitivity to the film orientation, to the strain and to the phase transitions which are intimately linked to specific phonon modes [13–16].

In this work we present results of the X-ray diffraction (XRD) and Raman spectroscopy studies on epitaxial $BiCrO_3$ (BCO) thin films fabricated by pulsed laser deposition on $(LaAlO_3)_{0.3}$-$(Sr_2AlTaO_6)_{0.7}$ (100)-oriented and $NdGaO_3$ (110)-oriented single crystal substrates.

2. Experimental details

The epitaxial BCO thin films were grown by pulsed laser deposition on (100)-oriented $(LaAlO_3)_{0.3}$-$(Sr_2AlTaO_6)_{0.7}$ (LSAT) and (110)-oriented $NdGaO_3$ (NGO) single crystal substrates. To optimize the epitaxial growth a 40 nm thick $La_{0.7}Sr_{0.3}MnO_3$ (LSMO) buffer layer onto LSAT and a 16 nm thick $SrRuO_3$ (SRO) buffer layer onto NGO has been grown. A KrF laser was used for ablation having a frequency of about 3–5 Hz and an effective energy of 2–3 J/cm². During the growth the substrates were heated up to ~650 °C under an oxygen partial pressure of 0.17–0.70 Pa. The target-to-substrate distance was 6 cm. A commercial $Bi_{1.1}CrO_3$ target (Pi-Kem Ltd.) with bismuth oxide excess, of 2 inch diameter, was employed for ablation.

The Raman spectroscopic measurements were carried out by a LabRam Horiba Jobin Yvon spectrometer using the frequency-doubled 532 nm excitation line of Nd:YAG laser. A backscattering geometry was employed with both incident and scattered light being perpendicular to the sample surface. Measurements were carried out at room temperature by rotating the sample azimuthally around the surface normal using both parallel (vv) and cross (hv) polarisation configurations in order to test the Raman selection rules. The scattered light was collected using a 100× magnification objective. To avoid any

* Corresponding author at: Leipziger Str. 23, D-09596 Freiberg, Germany. Tel.: +49 3731 39 2591; fax: +49 3731 39 4005.
E-mail address: andreas.talkenberger@tu-freiberg.de (A. Talkenberger).

0040-6090/$ – see front matter © 2011 Elsevier B.V. All rights reserved.
doi:10.1016/j.tsf.2011.10.196

influence of laser heating on the Raman spectra and to prevent damage on the surface of the samples, the laser power was reduced to ~0.6 mW.

The mutual crystallographic orientation between the film and the substrate was determined with the aid of pole figure measurements that were performed on a D8-Discover diffractometer from Bruker/AXS equipped with a general area detector diffraction system. During the pole figure measurement, the intensities diffracted both by the $NdGaO_3$ substrate and by the $BiCrO_3$ thin film were recorded as a function of the diffraction angle (2θ), the sample inclination from its symmetrical position (ψ) and the sample rotation around its (surface) normal direction (ϕ). The measured intensity maxima were plotted in form of the stereographic projection [17]. The 2D detector allowed a simultaneous data acquisition at different diffraction angles, which speeded up the search for the diffraction maxima in possibly strained epitaxially grown films. For the pole figure measurements CoKα radiation was used ($\lambda = 0.178897$ nm). High-resolution XRD (HR-XRD) measurements were carried out on an URD6 diffractometer at 0.154056 nm ($CuK\alpha_1$ radiation). The URD6 diffractometer was equipped with two perfect (111)-oriented dislocation-free silicon single crystals; one used as monochromator in the primary beam, the other as analyser in front of a scintillation detector.

3. Results and discussion

The epitaxial relation between the BCO film and the NGO substrate covered with the SRO buffer was concluded from the pole figure measurements using the procedure described in references [18, 19]. The pole figures measured for the NGO substrate at the detector angles 26.6° and 38.3° were overlaid and are shown in form of the stereographic projection in Fig. 1a. The detector angle is equal to the diffraction angle (2θ) in the middle of the detector area. Because of a large angular acceptance of the 2D detector, the XRD lines (020), (112) and (200) of the orthorhombic NGO, that are located at $2\theta = 37.954°$, 38.295° and 38.514° [20], respectively, were recorded simultaneously.

Likewise, the overlaid pole figures of the monoclinic BCO thin film that were measured at the detector angles 26.6°, 38.0° and 47.0° are displayed in Fig. 1b. The comparison of the pole figures from Fig. 1b with the stereographic projections of BCO having the space group C2/c [8] helped us to assign the individual diffraction maxima. Like for the NGO substrate, diffraction maxima from lattice planes with different interplanar spacings and thus with different diffraction angles were recorded simultaneously because of the large angular acceptance of the 2D detector. For the monoclinic BCO film this concerns the diffraction lines (202) with $2\theta = 37.528°$, (−113) with $2\theta = 37.814°$, (020) with $2\theta = 38.100°$, (31–1) with $2\theta = 38.189°$, (004) with $2\theta = 46.364°$, (400) with $2\theta = 46.998°$ and (−222) with $2\theta = 47.162°$. Because of the proximity of the diffraction angles of $(110)_{NGO}$ (26.780°) and $(111)_{BCO}$ (26.492°), these diffraction lines appear in both pole figures (Fig. 1a and b). The comparison of the stereographic projections of NGO and BCO, which were first oriented according to the measured and overlaid pole figures from Fig. 1, revealed that the lattice planes $(111)_{BCO}$ are nearly parallel to the lattice planes $(110)_{NGO}$. In the plane of the sample the nearly parallel crystallographic directions are $<-110>_{NGO}$ and $<10\text{–}1>_{BCO}$.

The upper part of Fig. 2 shows the monoclinic crystal system of BCO with the (111) and the (−11–1) planes being hatched. The epitaxial orientation relationship between BCO and NGO is displayed in the bottom part of Fig. 2. The pseudo-cubic axes of BCO correspond to the laboratory coordinates used for Raman measurements. It should be mentioned that the thickness of the BCO layer was 160 nm while the SRO buffer layer was only 16 nm thick, thus the SRO reflections were not considered during the pole figure measurement and the interpretation of the measured data.

In order to determine the orientation of the monoclinic BCO thin film grown on the (100)-oriented LSAT substrate coated with the LSMO buffer, symmetrical high resolution XRD measurement was

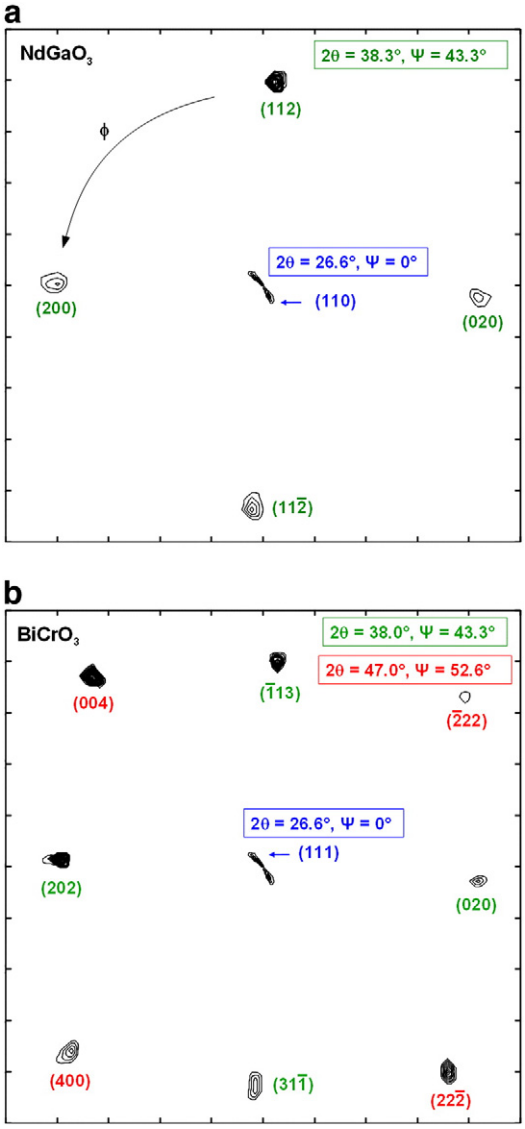

Fig. 1. Overlaid pole figures of the NGO substrate (a) and the epitaxially grown BCO film (b), measured at different detector angles (2θ). Angle ψ denotes the inclination of the diffraction vector from the sample surface perpendicular direction. The split central peak measured at $2\theta = 26.6°$ represents both the $(110)_{NGO}$ reflection and the monoclinic $(111)_{BCO}$ reflection.

performed. The presence of the XRD lines (111) from BCO and (100) from LSAT and the presence of the thickness oscillations in the HR-XRD pattern (Fig. 3) confirm that the BCO film has grown epitaxially on the LSAT substrate with the orientation $(111)_{BCO} \parallel (100)_{LSAT}$. The periodicity of the thickness oscillations corresponds to the thickness of the BCO layer of 80–90 nm. A high intensity of the thickness oscillations implies a (strained) epitaxial growth without relaxation, which is only possible for coherent epitaxial growth. The presence of the lattice strain and the absence of the lattice strain relaxation were confirmed by the shift of the diffraction line (111) of the monoclinic BCO from $2\theta = 22.76°$ (as calculated for $d_{111} = 0.3904$ nm in non-strained BCO) to $2\theta = 22.63°$. This difference in the diffraction angle corresponds to the out-of-plane lattice deformation ε of 5.65×10^{-3} as calculated using the differential form of the Bragg law,

$$\varepsilon = \frac{\Delta d}{d} = -\cot\theta \Delta\theta. \quad (1)$$

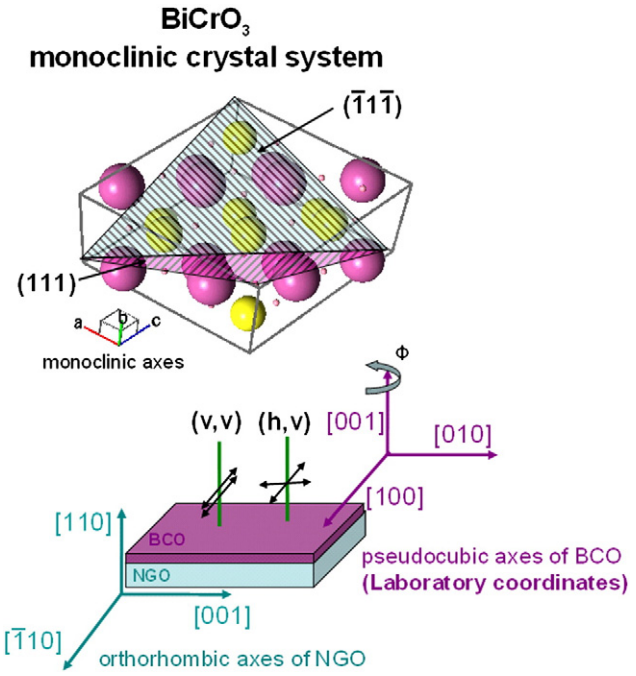

Fig. 2. Crystallographic orientation of monoclinic BCO (upper part) in respect to the crystal axes of orthorhombic NGO substrate (below). The big, middle, and small size balls correspond to the Cr, Bi, and O atoms, respectively. The hatched areas show the (111) and the (−11−1) monoclinic planes of BCO. The pseudocubic axes of BCO correspond to the laboratory coordinates used for the Raman measurements. The direction of the laser (corresponding to the [110] direction of NGO) and of the polarisations for (vv) and (hv) scattering configuration are also schematically shown.

This means that the in-plane lattice parameter of BCO fits to the lattice parameter of the substrate.

The laboratory coordinates used for the Raman measurements are the BCO pseudocubic coordinates as depicted in Fig. 2. The laser direction was parallel to the [110] direction of NGO. The azimuthal rotation of the sample was performed around this direction. The parallel (vv) and cross (hv) polarisation configurations are also schematically shown in Fig. 2. For the film grown on LSAT the situation is similar, the cubic axes of LSAT, being the same as the pseudocubic axes of BCO that represents the laboratory coordinate system.

The epitaxial orientation was also checked by performing polarisation-dependent Raman measurements. For these measurements the electric field vector of the incident laser beam was set either parallel to the field vector of the scattered light (vv) or perpendicular to it (hv). Additionally we rotated the sample azimuthally around its

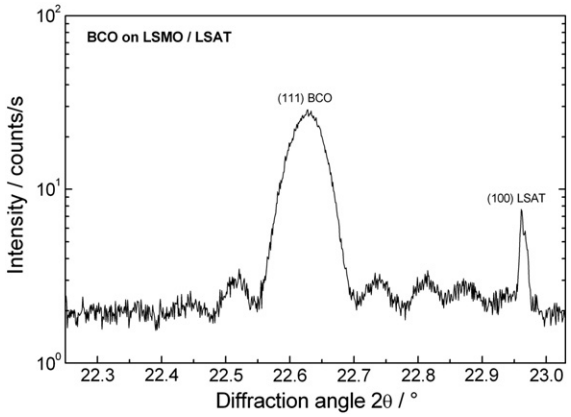

Fig. 3. Theta-2-theta HR-XRD pattern measured for an epitaxially grown BCO film on LSMO/LSAT substrate.

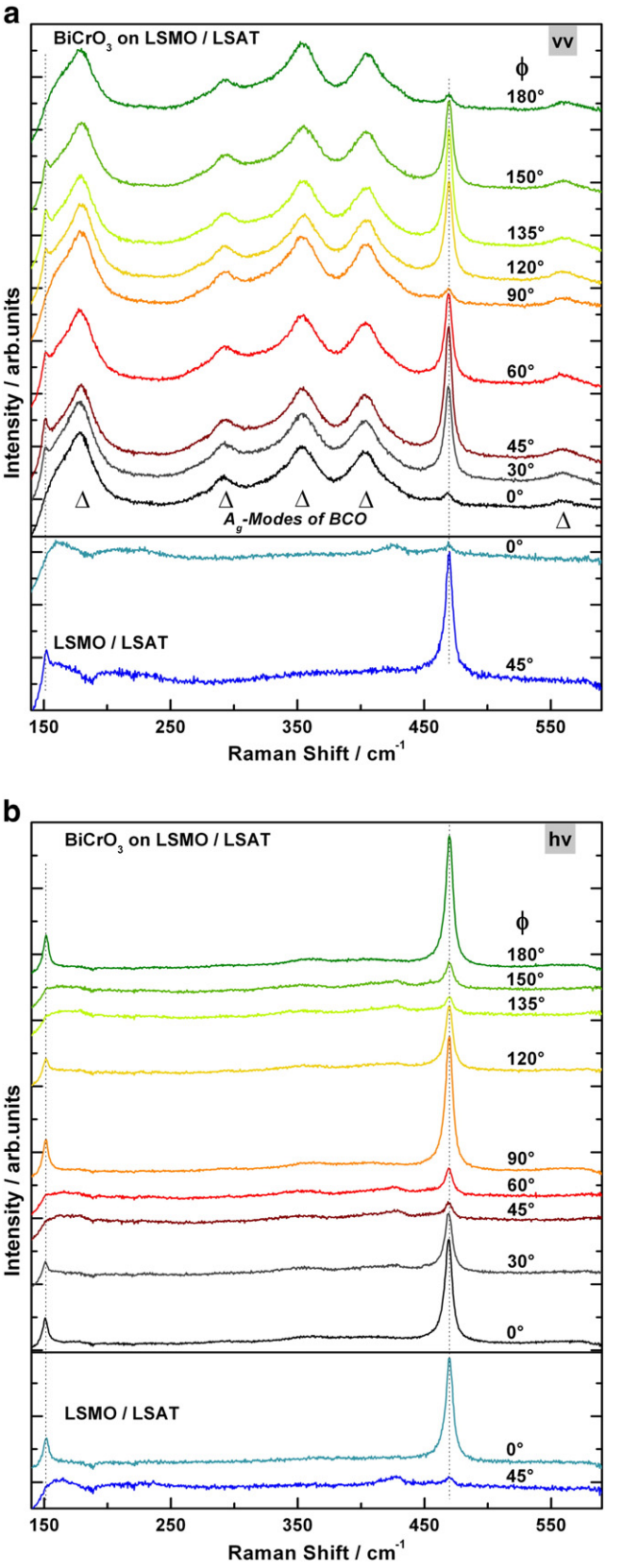

Fig. 4. a) Raman spectra of epitaxially grown BCO film on LSMO/LSAT substrate measured for different azimuthal angles ϕ (0°–180°) using parallel (vv) polarisation. Two representative spectra taken from LSMO/LSAT substrate are shown for comparison. Triangles symbolise the position of the strongest modes of BCO. b) Raman spectra of the same film and same substrate measured at the same azimuthal angles but for cross (hv) polarisation.

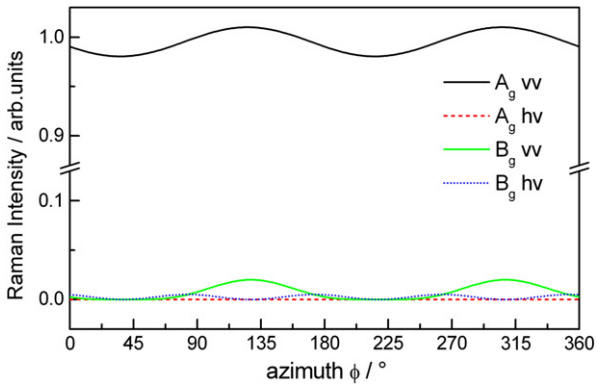

Fig. 5. Simulation of the A_g and B_g modes of BCO considering the C2/c space group for parallel and cross polarisation as function of azimuthal rotation angle with the tensor elements: $a=1$, $b=1$, $c=1$, $d=0.01$, $e=0.1$ and $f=0.1$.

normal (laser) direction. Fig. 4a shows the spectra measured in parallel polarisation configuration for different azimuthal angles for the BCO film deposited on LSMO/LSAT in the upper panel. In the bottom panel of Fig. 4a, we show for simplicity only two of the spectra of LSMO/LSAT measured for azimuthal angles of 0° and 45°. Part (b) of Fig. 4 shows the spectra for the same sample (upper panel), same substrate (down panel) and same rotation angle but measured in cross polarisation. The two peaks at 152 cm^{-1} and 470 cm^{-1} (marked by lines) correspond to the LSAT substrate and obey well the selection rules of a cubic crystal system showing a π/2 rotational symmetry. The Raman peaks at 179 cm^{-1}, 293 cm^{-1}, 354 cm^{-1}, 403 cm^{-1} and 559 cm^{-1} which belong to BCO [21], only appear in parallel polarisation configuration being completely absent in the spectra recorded in cross polarisation. Moreover the BCO peaks measured in the parallel configuration show nearly the same intensity independent on the azimuth angle. The same behaviour was also observed for the BCO film deposited on NGO. Here we present Raman data for the BCO film on LSAT because the Raman spectrum of LSAT is less complicated in comparison with that of NGO, so that the polarisation behaviour of BCO peaks can be observed more easily.

According to the factor group analysis [22] 60 vibrational modes are expected for BCO considering the monoclinic C2/c space group. 27 of these modes are Raman active (13 A_g+14 B_g). The Raman tensor of the A_g and B_g modes can be written as [23]:

$$A_g=\begin{pmatrix} a & 0 & d \\ 0 & b & 0 \\ d & 0 & c \end{pmatrix}, B_g=\begin{pmatrix} 0 & e & 0 \\ e & 0 & f \\ 0 & f & 0 \end{pmatrix} \quad (2)$$

For understanding the behaviour of the BCO Raman modes observed in the polarisation dependent measurements we simulate the behaviour of the A_g and B_g modes for both parallel and cross polarisation as a function of the azimuth angle. The scattered Raman intensity can be written using the following relation [24,25]:

$$I\sim\left|\mathbf{e_i}\mathbf{M}\mathbf{R}\mathbf{M}^{-1}\mathbf{e_s}\right|^2, \quad (3)$$

where $\mathbf{e_i}$ and $\mathbf{e_s}$ are the polarisation vectors for incident and scattered light, respectively. **M** is the Euler rotation matrix and **R** the Raman tensors as given by Eq. (2). In case of monoclinic symmetry, Raman tensors refer to a rectangular coordinate system where the monoclinic axis (in Fig. 3 it is b) coincides with the lattice basis. The other two directions, which are perpendicular to the monoclinic axis, can be chosen arbitrarily. There are several ways of deriving the coordinates of the polarisation vectors in the Raman tensor coordinate system. We have calculated the Euler rotation matrix **M** which rotates the normal to the (111) monoclinic plane into an [100] direction. The transpose of this matrix is then applied to the scattered polarisation direction. To investigate the effect of a rotation on polarisation, another free rotation angle around the [100] axis is included in the polarisation directions representing the azimuthal angle ϕ in the experiments. After these transformations the rotation matrix **M** has the following form:

$$\mathbf{M}=\begin{pmatrix} \cos[\phi]\ \cos[\psi]-\cos[\theta]\ \sin[\phi]\ \sin[\psi] & -\cos[\psi]\ \cos[\theta]\ \sin[\phi]-\cos[\phi]\ \sin[\psi] & \sin[\phi]\ \sin[\theta] \\ \cos[\psi]\ \sin[\phi]+\cos[\phi]\ \cos[\theta]\ \sin[\psi] & \cos[\phi]\ \cos[\psi]\ \cos[\theta]-\sin[\phi]\ \sin[\psi] & -\cos[\phi]\ \sin[\theta] \\ \sin[\psi]\ \sin[\theta] & \cos[\psi]\ \sin[\theta] & \cos[\theta] \end{pmatrix} \quad (4)$$

Thereby, ψ, θ and ϕ correspond to the Euler angles with ϕ representing the azimuthal angle.

For particular values of the tensor elements ($a=1$, $b=1$, $c=1$, $d=0.01$, $e=0.1$, $f=0.1$) the simulation of the A_g and B_g modes reproduce very well the experimentally observed behaviour. For a perfect cubic structure the off-diagonal elements of the Raman tensor are zero. In the simulations, the off-diagonal elements were set to be one order or two order of magnitudes smaller as the diagonal elements to account for the structural properties of the investigated perovskite. The monoclinic structure of BCO is in fact a slightly distorted cubic structure and can be indexed as pseudo-cubic. The slight distortion from the cubic symmetry is expected to induce off-diagonal elements that are significantly smaller than the diagonal elements.

The results of these calculations are shown in Fig. 5, where it can be seen that the A_g modes are appearing only in parallel polarisation, their intensity being nearly independent on the rotation angle, while the intensity in cross polarisation is very low. The B_g modes have a very low intensity in both cross and parallel configurations. These simulations clearly confirm the obtained experimental data indicating that the most intense Raman modes of BCO are the A_g ones while the B_g modes should have a weak intensity. For a complete determination of the tensor elements high quality single crystals of BCO are needed, which will allow Raman measurements scattered from different crystal planes.

4. Conclusions

High-resolution X-ray diffraction and XRD pole figure measurements have been performed in order to determine the epitaxial relationship between BCO thin films and NGO as well as LSAT substrates. It was found that the BCO films grow with the (111) monoclinic plane parallel to the substrate surface. Parallel and cross polarised Raman spectra for different azimuthal angles show that the BCO modes appear only in parallel configuration. These data were confirmed using symmetry based calculations, which indicate that the A_g modes appear only for parallel polarisation being independent of the azimuthal rotation angle.

Acknowledgements

This work is supported by the German Research Foundation (DFG) HI 1534/1-1. Kannan Vijayanandhini thanks the MPG-CNRS Program for Nanomaterials for supporting her work at MPI-Halle. Christian Röder thanks the Cluster of Excellence "Structure Design of Novel High-Performance Materials via Atomic Design and Defect Engineering (ADDE)" that is financially supported by the European Union (European regional development fund) and by the Ministry of Science and Art of Saxony (SMWK).

References

[1] Y.-H. Chu, L.W. Martin, M.B. Holcomb, M. Gajek, S.-J. Han, Q. He, N. Balke, C.-H. Yang, D. Lee, W. Hu, Q. Zhan, P.-L. Yang, A. Fraile-Rodríguez, A. Scholl, S.X. Wang, R. Ramesh, Nat. Mater. 7 (2008) 478.
[2] G. Catalan, J.F. Scott, Adv. Mater. 21 (2009) 2463.
[3] R. Ramesh, N.A. Spaldin, Nat. Mater. 6 (2007) 21.

[4] J. Wang, J.B. Neaton, H. Zheng, V. Nagarajan, S.B. Ogale, B. Liu, D. Viehland, V. Vaithyanathan, D.G. Schlom, U.V. Waghmare, N.A. Spaldin, K.M. Rabe, M. Wuttig, R. Ramesh, Science 299 (2003) 1719.
[5] H.W. Jang, D. Ortiz, S.-H. Baek, C.M. Folkman, R.R. Das, P. Shafer, Y. Chen, C.T. Nelson, X. Pan, R. Ramesh, C.-B. Eom, Adv. Mater. 21 (2009) 817.
[6] F. Sugawara, S. Iida, J. Phys. Soc. Jpn. 20 (1965) 1529.
[7] C. Darie, C. Goujon, M. Bacia, H. Klein, P. Toulemonde, P. Bordet, E. Suard, Solid State Sci. 12 (2010) 660.
[8] A.A. Belik, S. Iikubo, K. Kodama, N. Igawa, S. Shamoto, E. Takayama-Muromachi, Chem. Mater. 20 (2008) 11.
[9] A. David, P. Boullay, R.V.K. Mangalam, N. Barrier, W. Prellier, Appl. Phys. Lett. 96 (2010) 221904.
[10] M. Opel, S. Geprägs, E.P. Menzel, A. Nielsen, D. Reisinger, K.-W. Nielsen, A. Brandlmaier, F.D. Czeschka, M. Althammer, M. Weiler, S.T.B. Goennenwein, J. Simon, M. Svete, W. Yu, S.-M. Hühne, W. Mader, R. Gross, Phys. Status Solidi A 208 (2011) 2.
[11] N.A. Hill, P. Bättig, C. Daul, J. Phys. Chem. B 106 (2002) 13.
[12] D.H. Kim, Appl. Phys. Lett. 89 (2006) 162904.
[13] D.A. Tenne, X. Xi, J. Am. Ceram. Soc. 91 (2008) 1820.
[14] J. Kreisel, P. Bouvier, J. Raman Spectrosc. 34 (2003) 524.
[15] R. Palai, R.S. Katiyar, H. Schmid, P. Tissot, S.J. Clark, J. Robertson, S.A.T. Redfern, G. Catalan, J.F. Scott, Phys. Rev. B 77 (2008) 0140110.
[16] C. Himcinschi, I. Vrejoiu, M. Friedrich, E. Nikulina, L. Ding, C. Cobet, N. Esser, M. Alexe, D. Rafaja, D.R.T. Zahn, J. Appl. Phys. 107 (2010) 123524.
[17] L.V. Azároff, Elements of X-ray Crystallography, McGraw-Hill Book Company, New York, San Francisco, London, 1968, p. 28.
[18] D. Rafaja, J. Kub, D. Šimek, J. Lindner, J. Petzelt, Thin Solid Films 422 (2002) 8.
[19] P. Kuppusami, G. Vollweiler, D. Rafaja, K. Ellmer, Appl. Phys. A 80 (2005) 183.
[20] PDF2 database on CD-ROM, ICDD Newtown Square, PA, USA, 2003.
[21] C. Himcinschi, I. Vrejoiu, T. Weißbach, K. Vijayanandhini, A. Talkenberger, C. Röder, S. Bahmann, D.R.T. Zahn, A.A. Belik, D. Rafaja, J. Kortus, J. Appl. Phys. 110 (2011) 073501.
[22] D.L. Rousseau, R.P. Bauman, S.P.S. Porto, J. Raman Spectrosc. 10 (1981) 253.
[23] R. Loudon, Adv. Phys. 50 (2001) 813.
[24] G. Turell, J. Raman Spectrosc. 15 (1984) 103.
[25] V. Pajcini, S.A. Asher, J. Am. Chem. Soc. 121 (1999) 10942.